Supporting Information

Thermally-induced crystal-to-crystal transformations accompanied by changes in the magnetic properties of a Cu^{II}-*p*-Hydroquinonate Polymer.

Ngoc Hien Phan, Ivan Halasz, Ingo Opahle, Edith Alig, Lothar Fink, Jan W. Bats, Pham Thanh Cong, Hans-Wolfram Lerner, Biprajit Sarkar, Bernd Wolf, Harald O. Jeschke, Michael Lang, Roser Valentí, Robert Dinnebier, and Matthias Wagner

1. Differential Thermal Analysis (DTA) and Thermogravimetric Analysis (TGA) of compound 1

Crystals of **1** (32.29 mg) were placed in an alumina crucible and heated to a temperature of 200 °C (rate: 5 °C min^{-1}; DTA/TGA analyser Setaram TGA-92) under an atmosphere of N_2 (flow rate of N_2: approx. 1.5 L h^{-1}). The DTA/TGA curves obtained are shown in Figure 1S.

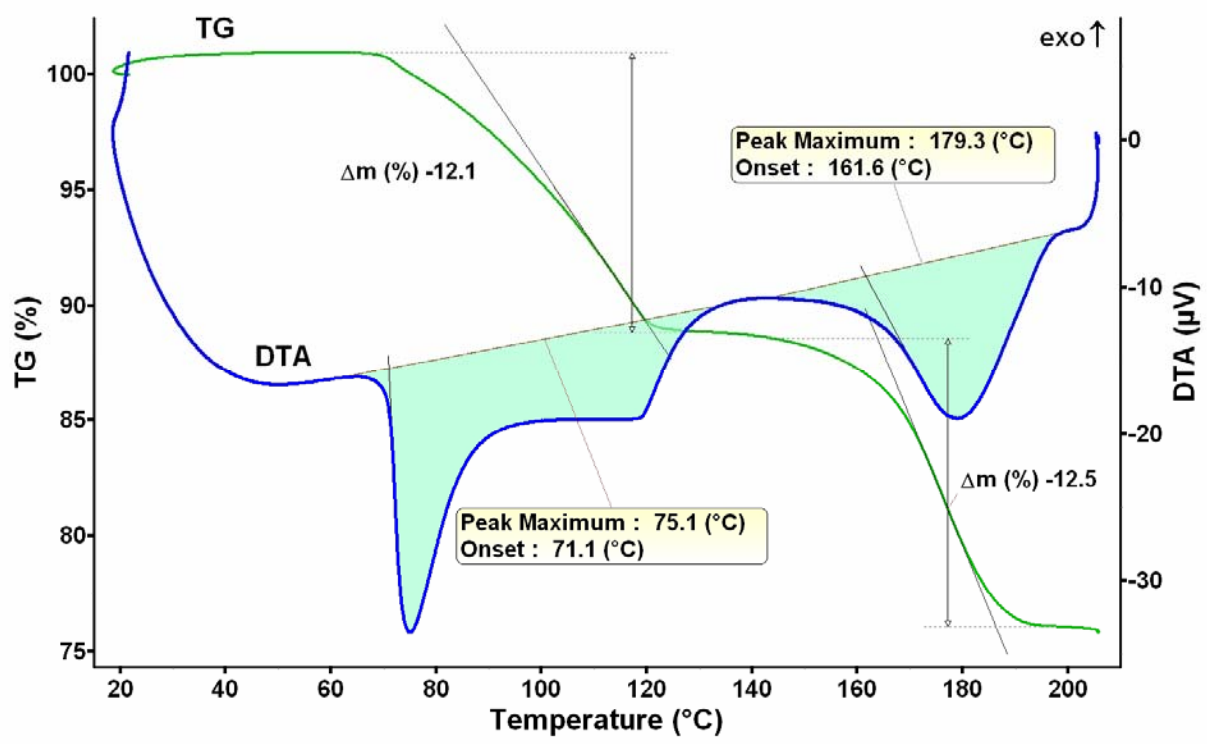

Figure 1S. DTA/TGA curves of a sample of **1** (gentle grinding; heating rate: 5 °C min^{-1}).

2. Synthesis of 2 and 3; X-ray powder diffractograms of bulk samples of compounds 1 and 2

Compound 2. To obtain a sample of **2** for elemental analysis, finely ground crystals of **1** were heated in the DTA/TGA analyser (see above) to a temperature of 110 °C until the sample mass remained constant (Found: C, 38.45; H, 3.93; N, 9.37; S, 6.70. Calc. for $C_{30}H_{34}Cu_2F_6N_6O_{10}S_2$ (943.83): C, 38.18; H, 3.63; N, 8.90; S, 6.79%).

For X-ray crystallography, a carefully selected crystal of **1** (7.686 mg) was placed in an alumina crucible and slowly heated to 85 °C (rate: 5 °C min^{-1}) under an atmosphere of N_2 in a DTA/TGA analyser (Setaram TGA-92). The crystal was kept at 85 °C for 1 h, then cooled to rt (rate: 5 °C min^{-1}) and investigated by single crystal X-ray diffraction.

Compound 3. To obtain a sample of **3** for elemental analysis, finely ground crystals of **1** were heated in the DTA/TGA analyser (see above) to a temperature of 220 °C until the sample mass remained constant (Found: C, 36.45; H, 2.53; N, 6.94. Calc. for $C_{24}H_{20}Cu_2F_6N_4O_8S_2$ (797.66): C, 36.14; H, 2.53; N, 7.02%).

For X-ray crystallography, a sample of **1** was gently ground in an agate mortar yielding a fine red-brown powder and packed in a 0.5 mm diameter borosilicate glass capillary. The capillary was left open on one side to allow for the DMF to diffuse out of the capillary during heating. The sample was first heated to 100 °C (rate: 0.1 °C s^{-1}) and formation of **2** was confirmed. Afterwards, the sample was heated to 220 °C (rate: 0.1 °C s^{-1}) and quick powder patterns were collected until they stopped changing. The capillary was then cooled to room temperature (rate: ~0.5 °C s^{-1}) for the collection of a high quality pattern of **3**, which was used in the structure solution procedure and for Rietveld refinement.

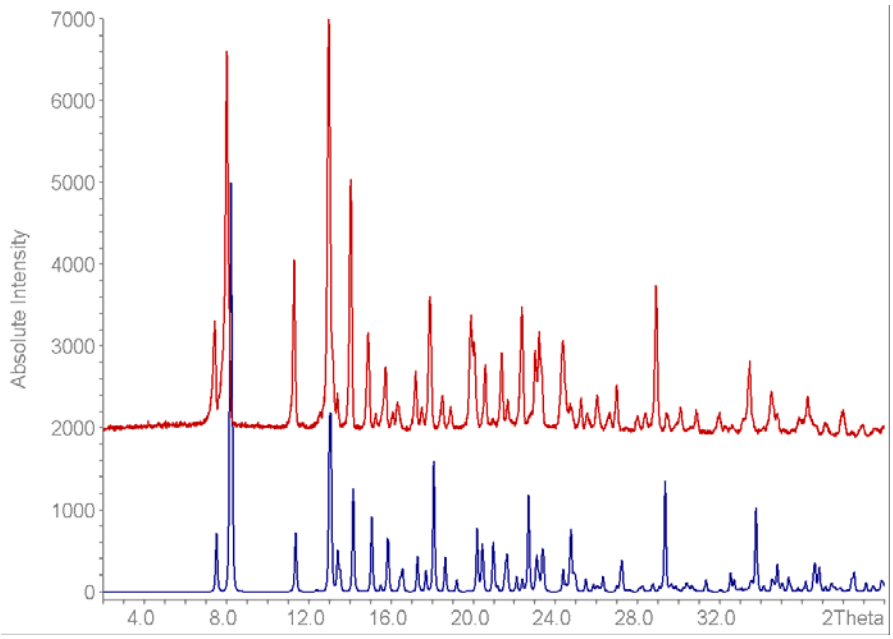

Figure 2S. X-ray powder diffractogram of compound **1** measured at 293 K (red line); simulated X-ray powder diffractogram from single crystal data of **1** (data acquired at 155 K; cf. Ref. [12]).

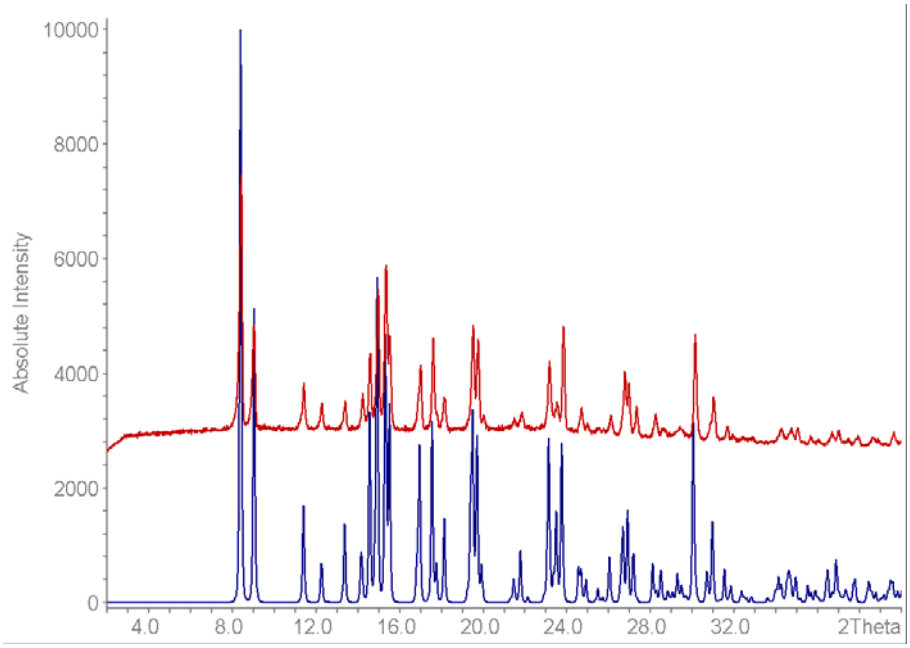

Figure 3S. X-ray powder diffractogram of compound **2** measured at 193 K (red line); simulated X-ray powder diffractogram from single crystal data of **2** (data acquired at 164 K; this work).

3. X-ray single crystal structure analysis of 2

A single crystal (black rod with dimensions 0.26 × 0.34 × 0.75 mm) was measured on a SIEMENS SMART CCD diffractometer with graphite-monochromated MoK_α radiation. Repeatedly measured reflections remained stable. The crystal was of poor quality with broad and slightly split reflection profiles (peak widths between 2° and 4°). An empirical absorption correction with program SADABS[1] gave a correction factor between 0.33 and 0.71. Equivalent reflections were averaged. Friedel opposites were not averaged. The structure was determined by direct methods using program SHELXS[2]. All H atoms were geometrically positioned and constrained. The structure was refined with full-matrix least-squares on F^2 using the program SHELXL-97[3]. The value of the Flack parameter was x = 0.49(2) and showed the crystal to be an inversion twin.

1 G. M. Sheldrick, *SADABS*, University of Göttingen, Germany, 2000. 2 Sheldrick, G. M. *Acta Cryst.* 1990, **A46**, 467. 3 Sheldrick, G. M. *SHELXL-97. A Program for the Refinement of Crystal Structures*, University of Göttingen; Göttingen, Germany, 1997.

Crystal data: $C_{30}H_{34}Cu_2F_6N_6O_{10}S_2$, M_r = 943.83, monoclinic, space group $P2_1$, a = 7.8327(16) Å, b = 19.556(4) Å, c = 12.624(3) Å, β = 97.82(3)°, V = 1915.7(7) Å^3, Z = 2, ρ_{calcd} = 1.636 g cm^{-3}, μ = 1.309 mm^{-1}, λ = 0.71073 Å, T = 164(2) K, 23637 measured reflections, 7380 unique (R_{int} = 0.1415), $R1[I>2\sigma(I)]$ = 0.0783, $wR2[I>2\sigma(I)]$ = 0.1564, GoF = 0.998, 509 parameters / 37 restraints, final difference map within −1.10 and +1.06 eÅ^{-3}.

4. X-ray powder structure analysis of 3

The high quality X-ray powder diffraction pattern, which was used in the structure solution procedure and for Rietveld refinement, was collected in a 2θ region from 5° to 65° with steps of 0.0085°; the total data collection time was 18 h. High resolution powder diffraction patterns were collected on a laboratory diffractometer (Bruker D8 ADVANCE with Våntag-1 position sensitive detector with a 6° opening angle and Cu$K\alpha_1$ radiation from primary Ge(111)-Johansson-type monochromator) in Debye-Scherrer geometry. The capillary was rotated during data collection for better particle statistics. The diffractometer is equipped with a capillary furnace (MRI Physikalische Geräte GmbH, Karlsruhe) for temperature-resolved XRPD measurements.

Indexing of the powder pattern was performed using the program Topas[1] and $P2_1/c$ was determined as the most likely space group. Considering the volume of the unit cell, the asymmetric unit needs to consist of a half of the bridging ligand with one copper atom and one triflate counterion. These structure fragments were taken from the solved structure of **1** and introduced into simulated annealing global optimization which was performed with the program Fox[2]. Bond lengths and bond angles were restrained to the values taken from compound **1**, but all torsion angles were allowed to be optimized. The position of the triflate ion was optimized independently from the position of the metal-containing fragment. The likely initial model was recognized when the six-membered ring (central in the ligand) assembled over an inversion center and a triflate oxygen atom came close to the copper atom. Also, no prohibitively close contacts were present. This model was introduced into Rietveld refinement (Figure 4S) which was performed with the program Topas[1] using restraints on bond lengths and angles as well as some planarity restraints.

Given that the Cu−O−Cu bond angle in **3** is particularly important with regard to the magnetic interaction of the Cu^{II} ions, this parameter was finally varied in the interval between 95° and 110°; the best Rietveld fit was achieved for Cu−O−Cu = 104.6(1)°. The final structure model was obtained during extensive testing against the measured powder pattern by performing a search in the parameters' space in the vicinity of the initial structural model. A series of refinement cycles (more than several hundreds) was undertaken in such a way that, after each refinement cycle achieved convergence, values of all the atomic coordinates were changed by adding a small random number (between –0.008 and 0.008 in fractional coordinates) and used as new starting values in the next refinement cycle. Such refinements resemble simulated annealing within a narrow region of parameters' space where the geometry restraints "put the

molecular structure back" after randomization of atomic coordinates. Thus, by setting geometry restraints to values expected in the case **3** contained Cu^{I}, and, conversely, in case it contained Cu^{II} (differences being also in the *p*-hydroquinone fragment), it was confirmed that this geometry indeed gives the best fit to the measured powder pattern. Such runs can be performed in an automated way with Topas.[1]

1 Topas, version 4.1 Bruker AXS, Karlsruhe, Germany. 2 V. Favre-Nicolin, R. Černý *J. Appl. Cryst.* 2002, **35**, 734.

Crystal data: $C_{24}H_{20}Cu_2F_6N_4O_8S_2$, M_r = 797.66, monoclinic, space group $P2_1/c$, a = 10.9255(2) Å, b = 7.9649(1) Å, c = 18.3689(3) Å, β = 116.075(1)°, V = 1435.78(4) Å^3, Z = 2, ρ_{calcd} = 1.8451(1) g cm^{-3}, λ = 1.54059 Å, T = 293(2) K, R_{exp} = 1.78, R_p = 3.18, R_{wp} = 2.41, $R(F^2)$ = 1.24, GoF = 1.78, 150 parameters, starting angle (2θ) = 3°, final angle (2θ) = 65°, step width (2θ) = 0.00853°.

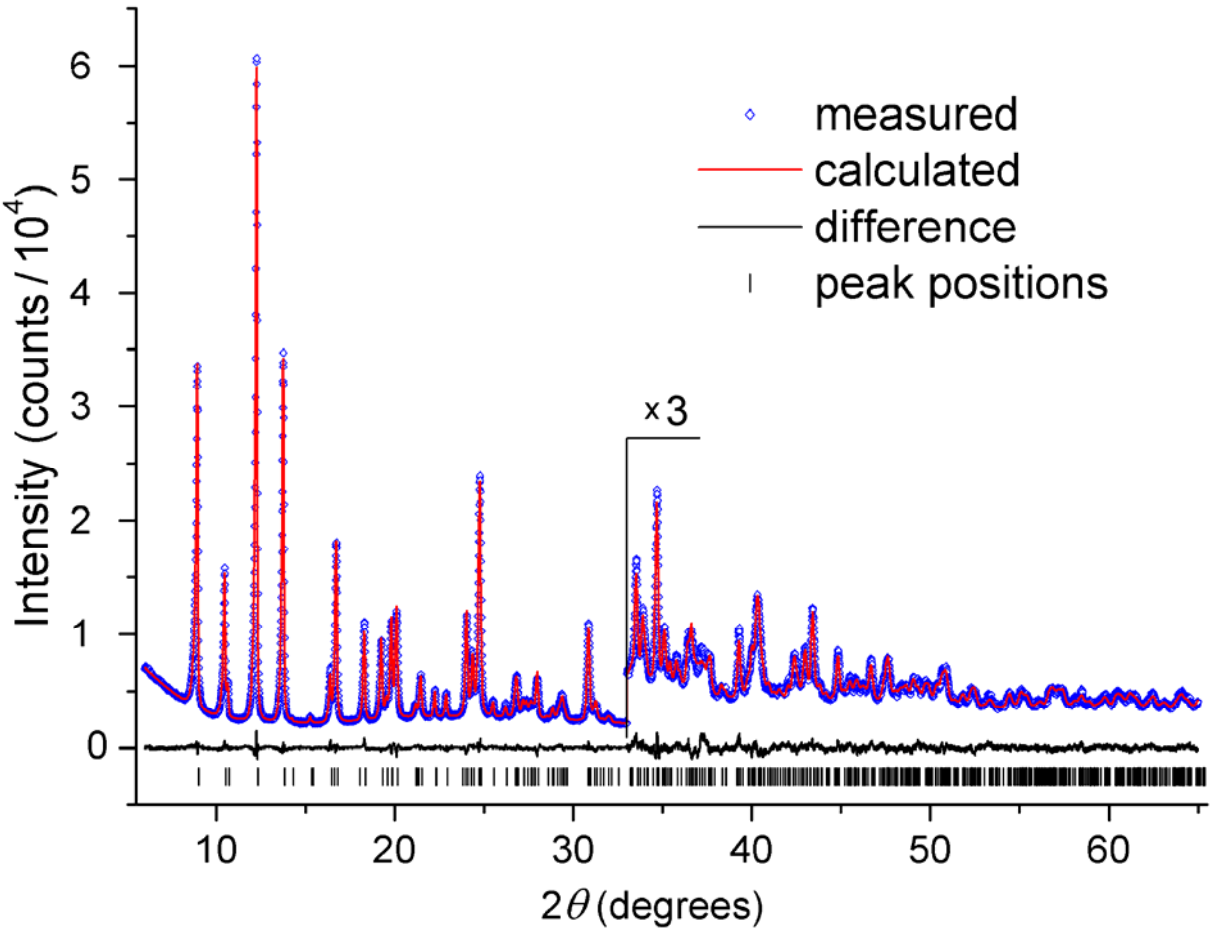

Figure 4S. Final Rietveld plot of **3**.

5. Magnetic susceptibility measurements on 1, 2, and 3

The magnetic susceptibilities of **1**, **2** and **3** were measured in the temperature range between $2\ \mathrm{K} \leq T \leq 300\ \mathrm{K}$ and in a magnetic field of $B = 1\ \mathrm{T}$ using a Quantum Design SQUID magnetometer (sample weights: **1**: 12.30 mg; **2**: 26.56 mg; **3**: 30.64 mg). The measurements on **1** were performed on small single crystals with the external field oriented perpendicular to the crystallographic *a*-axis. An array of tiny single crystals was used for **2** and a microcrystalline powder sample for **3**. In both cases, the field was randomly oriented with respect to the crystal axes. The data of all three compounds were corrected for the temperature-independent diamagnetic core contribution, according to Ref[1], and the magnetic contribution of the sample holder. The latter, determined from an independent measurement, is displayed through solid black circles in the main panel and the inset of Figure 5S. As is clearly visible, the magnetic moment of the sample holder consists of at least two parts: a large temperature-independent diamagnetic contribution and a small Curie-Weiss-like paramagnetic one. The latter gives rise to an upturn of the magnetic moment of the sample holder below 10 K. A careful determination of the magnetic background is of crucial importance, especially for the analysis of the weak magnetic signal of **3**. The raw data are displayed as solid black squares in the inset. The signal is diamagnetic down to approximately 80 K. The open squares in Figure 5S are the experimental data of **3** corrected for the contribution of the sample holder. As clearly shown in the inset, the diamagnetic contribution is governed by the magnetic background. The experimental data exhibit a marked upturn below 20 K, indicating the presence of a small concentration of paramagnetic centres. In fact, a fit based on a Curie-Weiss model (blue solid curve in Figure 5S) for $T \leq 300$ K provides an excellent description of the data up to 150 K. The fit yields a concentration of approximately 6% of nearly uncoupled ($\Theta_{CW} = -0.28$ K) spin $S = ½$ entities. By assigning this paramagnetic contribution to magnetic impurities, which are likely to result from magnetically nearly uncoupled Cu^{II} centers formed by the breakdown of some coordination polymer chains during heat treatment, the intrinsic magnetic moment of **3** is obtained by subtracting this Curie-Weiss contribution from the measured data (black open squares).

1 O. Kahn, *Molecular Magnetism* **1993**, New York: Wiley-VCH

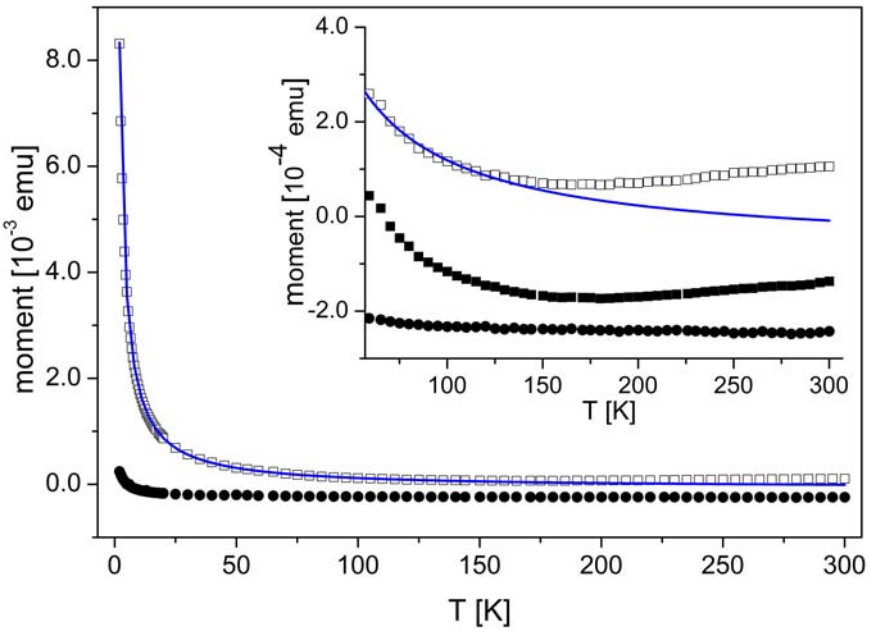

Figure 5S. Magnetic moment of **3** as a function of temperature (black open squares) after subtraction of the magnetic contribution of the sample holder (black solid circles). The data were measured in a field of 1 T using a sample of 30.64 mg of **3**. The solid blue line corresponds to a Curie-Weiss fit yielding a contribution of approximately 6 % uncoupled Cu^{2+} ions. Inset: Blow-up of the curves shown in the main panel for 60 K $\leq T \leq$ 300 K together with the raw experimental data (black solid squares).

6. Electron paramagnetic resonance spectroscopy on 1, 2, and 3

EPR spectra in the X band were recorded with a Bruker System EMX connected with an ER 4131 VT variable temperature accessory. The measurements were carried out on powder samples of **1** and **2**.

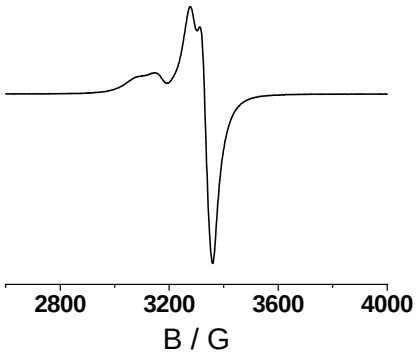

Figure 6aS. EPR spectrum of compound **1**. $g(\parallel) = 2.166$; $g(\perp) = 2.072$.

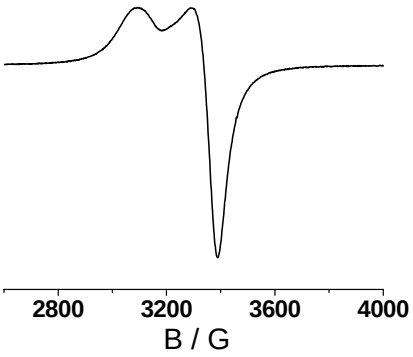

Figure 6bS. EPR spectrum of compound **2**. $g(\parallel) = 2.239$; $g(\perp) = 2.062$.

Note: The expected hyperfine splitting in case of **1** and **2** due to the nuclear spin of Cu ($I(^{63,65}\mathrm{Cu}) = 3/2$) is not well resolved.[1] Compound **3** is EPR silent.

1 S. Güner, M. K. Şener, H. Dinçer, Y. Köseoğlu, S. Kazan, M. B. Koçak, *J. Magnetism Magnet. Mater.* 2006, **300**, e530.

7. Infrared spectra of 1, 2, and 3

The spectra were measured on a Jasco FT/IR-4200 spectrometer.

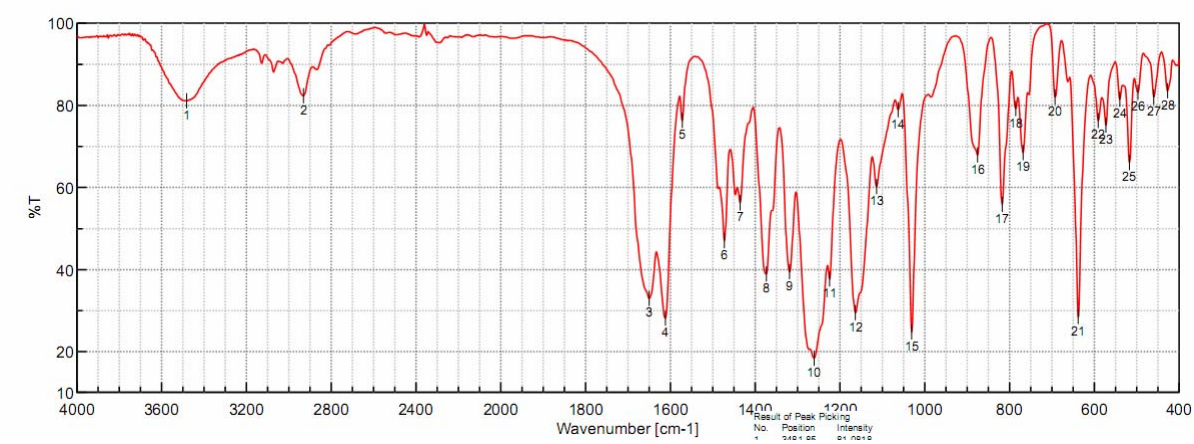

Figure 7aS. Infrared spectrum of compound **1** (KBr). No 3: 1650 cm^{-1}; 4: 1612 cm^{-1}.

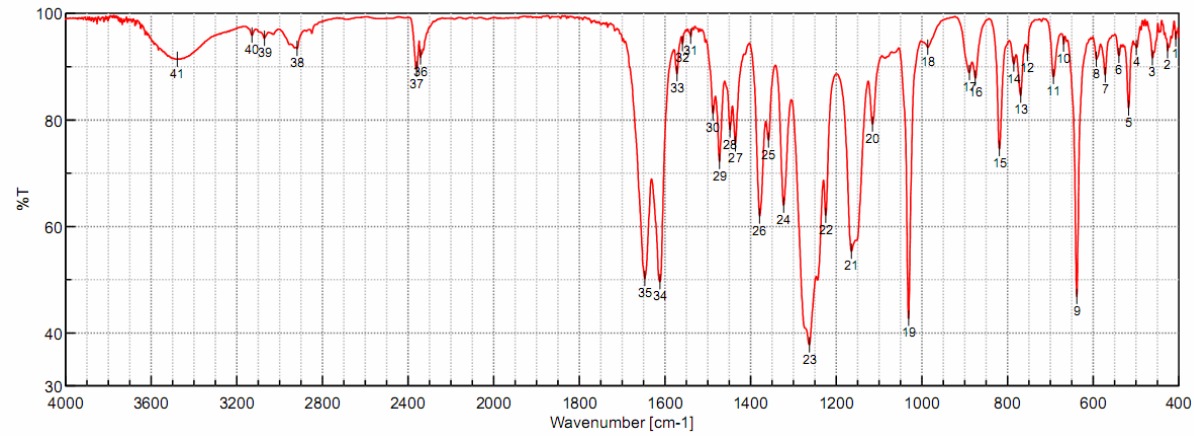

Figure 7bS. Infrared spectrum of compound **2** (KBr). No 35: 1647 cm^{-1}; 34: 1612 cm^{-1}.

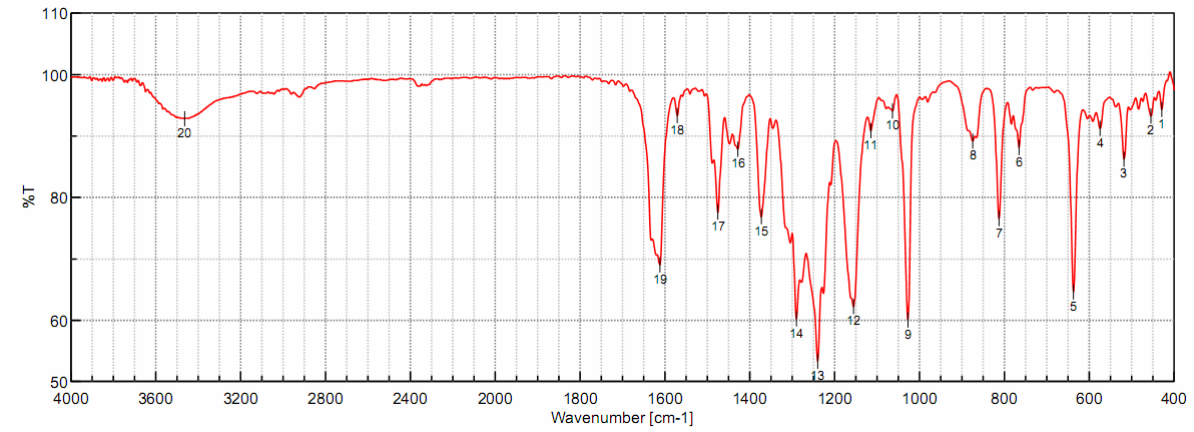

Figure 7cS. Infrared spectrum of compound **3** (KBr). No 19: 1612 cm^{-1}.

Infrared spectra of **1**, **2**, and **3** were run on KBr pellets. The spectra closely resemble each other with the exception of the wavenumber intervals between (i) 1700 – 1600 cm^{-1} (region of the CO stretch of DMF) and (ii) 1400 – 1200 cm^{-1} (region of triflate absorptions): (i) **1** gives rise to a very broad band at $\tilde{\nu}$ = 1650 cm^{-1}, which becomes considerably sharper in the case of **2** and essentially vanishes in the IR spectrum of **3**. This feature is in accord with a gradual loss of DMF ligands along this series of compounds. (ii) The IR spectra of **1** and **2** are similar in the spectral region between 1400 and 1200 cm^{-1}. However, substantial changes in the absorption pattern are evident for **3**, which can be explained by the presence of separated ions in **1** / **2** as opposed to contact ion pairs in **3**.

8. UV/vis spectra of 1, 2, and 3

The spectra were measured on a Varian Cary 50 Scan spectrometer. The solid-state spectra were recorded by dusting a fine powder of the respective compound onto Scotch tape, which was then fixed to the wall of a quartz cuvette.

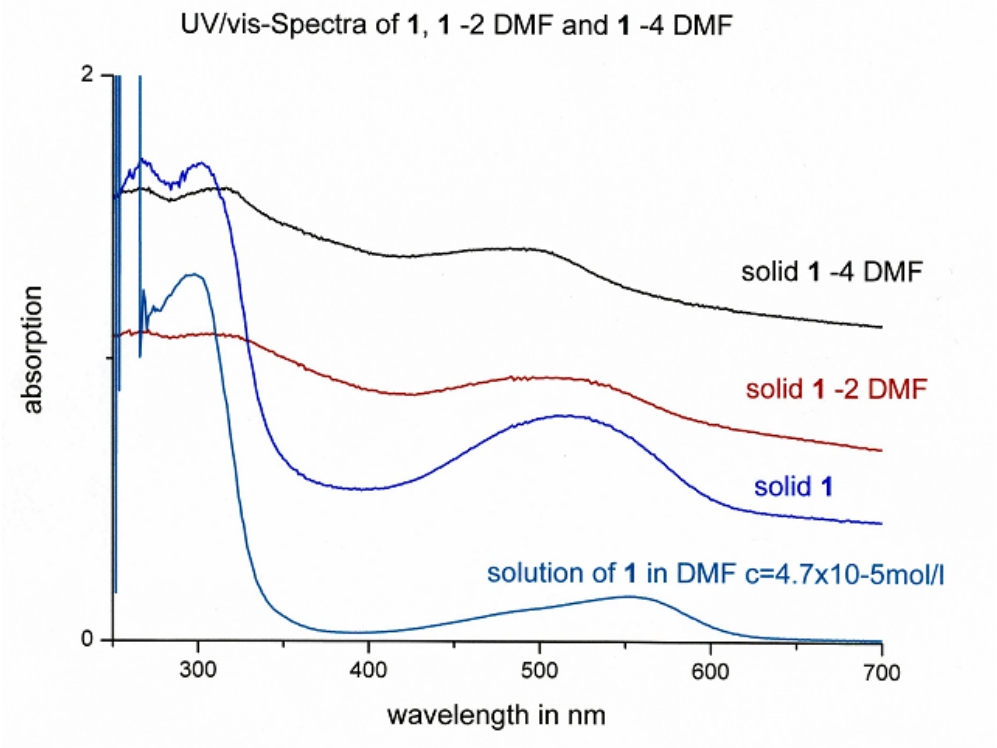

Figure 8S. UV/vis spectra of **1** (DMF solution and solid state), **1**−2DMF (= **2**; solid state), and **1**−4DMF (= **3**; solid state).

The UV/vis spectra of **1** (DMF solution and solid state), **2** (solid state), and **3** (solid state), are qualitatively similar and thus indicate the electron distribution in all three compounds to be pretty much alike.

9. DFT calculations on 3

The electronic structure of **3** was calculated in the framework of density functional theory (DFT). The calculations were performed with the full potential local orbital method (FPLO, version 9.00-33)[1] in the scalar relativistic approximation. The Perdew-Wang[2] parameterization of the exchange-correlation potential in the local (spin-)density approximation (L(S)DA) was used. In addition, the effect of strong onsite Coulomb correlations was taken into account employing the LSDA+U formalism[3]. Here, both the Atomic Limit (AL) and the Around the Mean Field (AMF) functionals have been used. Exchange constants were obtained by mapping total energy differences of cells with different spin arrangements onto a Heisenberg model. Convergence of the exchange constants with respect to **k**-space integrals was tested with 8 and 64 **k**-points in the full Brillouin zone, showing a convergence of the energy differences better than 15 K.

1 K. Koepernik, H. Eschrig *Phys. Rev. B* 1999, **59**, 1743; **http://www.FPLO.de**. 2 J. P. Perdew, Y. Wang *Phys. Rev. B* 1992, **45**, 13244. 3 H. Eschrig, K. Koepernik, I. Chaplygin *J. Solid State Chem.* 2003, **176**, 482.